Progress In Electromagnetics Research, Vol. 125, 79–95, 2012

ESTIMATION METHOD FOR SIMULTANEOUS SWITCHING NOISE IN POWER DELIVERY NETWORK FOR HIGH-SPEED DIGITAL SYSTEM DESIGN

T.-H. Ding*, Y.-S. Li, D.-C. Jiang, Y.-Z. Qu, and X. Yan

School of Electronic Engineering, Xidian University, No. 2 South Taibai Road, Xi'an, Shaanxi 710071, China

Abstract—In this paper, a new method is proposed to estimate the simultaneous switching noise (SSN) directly from the power delivery network (PDN) frequency-domain impedance in order to reduce the time-domain simulation of SSN and computational burden, which is based on the periodic characteristics of the switching current and the SSN produced by one current pulse. The frequency-domain impedance is approximated with several single resonance circuits, which can capture the resonance characteristics of the PDN. The parameters of each resonance circuit are calculated with the rational function. It is also found that the SSN can be suppressed through adjusting the resonant frequencies and the period of switching current. Compared with the single resonance lumped circuit model and multi-resonance distributed circuit model, the performance of the new method for estimating the SSN is verified, which is more accurate than the target impedance method.

1. INTRODUCTION

As clock frequency and chip integration levels increase in a digital system, simultaneous switching noise generated on the power delivery network of printed circuit boards (PCBs) and packages can limit performance [1, 2]. SSN, also known as power/ground bounce noise or delta-I noise, on the power/ground bus has become one of the major concerns in the design of high-speed digital circuit systems with even faster edge rates, lower voltage levels and higher integrations. The SSN mainly attributes to three reasons, inductance of non-ideal signal path, mutual inductive coupling of PDNs and power supply compression.

Received 12 January 2012, Accepted 12 February 2012, Scheduled 20 February 2012

* Corresponding author: Tong-Hao Ding (dingtonghao1985@126.com).

In particular, the SSN in a wide frequency range incidentally excites multiple resonance modes between the power/ground planes as in the parallel planes model, which would also introduce significant signal integrity problems, power integrity issues, and electromagnetic interference (EMI) [3–5]. If the SSN exceeds the noise margin, the IC may experience a functional failure.

To ensure the success in the modeling of SSN, equivalent circuit extraction techniques are adopted to model the behavior of PDNs at high frequencies. PCBs, voltage regulator modules (VRM) and many types of capacitors are included in a PDN with special structures. How to model the PDN including different types of modules with wideband features, and at the same time possess rather complicated coupling schemes, is a very challenging task by the conventional approaches. The modeling methods have been discussed in many papers, numerical methods such as method of moments (MoM), finite-difference method (FDM) and finite difference time domain (FDTD) have been used in the past to analyze the PCB structures [6–13]. The transmission matrix method (TMM) uses a fast method of computing the port-to-port behavior of special parallel plane structures based on the transmission matrix (or ABCD matrix) of each column of unit cells [14]. The partial equivalent electric circuit (PEEC) method is widely used to model complex three-dimensional structures, which has also been extended with retardation to provide a full-wave solution.

One of the challenges of PDN design is to provide clean power to electronics when a surge current occurs, so the suppression of SSN on a multilayer PCB is a critical task in system design to ensure signal integrity and to reduce the risk of EMI problems. To address the SSN issue, several techniques have been proposed in previous works. Decoupling capacitors are used to realize low impedance in frequency domain and the number of capacitors on a PC should be minimized from a cost point of view. Hence, the proper number of decoupling capacitors, and the proper value of the decoupling capacitors should be chosen carefully [15, 16]. Electromagnetic band-gap (EBG) structures are proposed to suppress the SSN in GHz range because of their high-impedance planes, however signal integrity is degenerated by periodic EBG structures, because the periodic structures on the power plane seriously affect the return path, and the applications of EBG in the package and chip need to be studied [17–20]. Power islands are commonly used to isolate devices that put noise on a power bus from devices that may be susceptible to power bus noise, and bridges are also used to connect two sides of the slit to maintain the signal integrity of transmission lines crossing the slit, which degrades the capability of the SSN suppression significantly [21, 22].

The investigation of PDN design is mainly done in frequency domain, so the time-domain response of the PDN is neglected because the transient characteristics of SSN produced by one current pulse and switching current are not considered. Generally, the worst case and the best case of SSN are important parameters for PDN design, so a new estimation method is proposed to evaluate the largest and the smallest SSN magnitudes based on the periodic characteristics of the switching current and the SSN produced by one current pulse in this paper. It is found that the SSN would accumulate based on the period of switching current. The periods of the SSN produced by one current pulse are mainly determined by resonant frequencies, so the PDN impedance is approximated with several single resonance circuit models to capture the resonance characteristics, and the worst case and the best case of the SSN are obtained to evaluate the performance of the PDN. The performance of the new method is verified with the single resonance lumped circuit model and multi-resonance distributed circuit model, which can obtain more accurate results than the target impedance method.

2. ESTIMATION OF THE SIMULTANEOUS SWITCHING NOISE

2.1. SSN Estimation of the Single Resonance Circuit

The schematic diagram of SSN suppression and transmission is shown in Fig. 1, where PCBs, voltage regulator modules (VRM) and many types of capacitors are included in the PDN. The input impedance

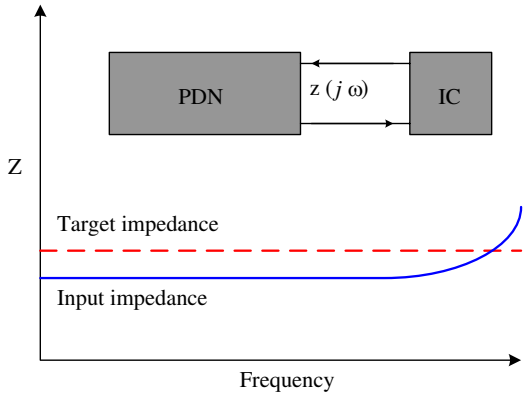

Figure 1. Schematic diagram of the target impedance.

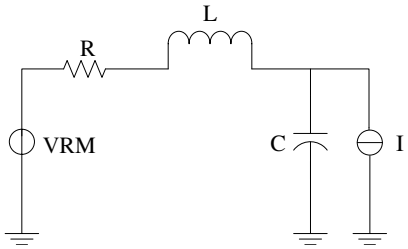

Figure 2. Single resonance circuit model.

$Z(j\omega)$ should be lower than the target impedance Z_T for noise voltage less than the allowed ripple on the power supply when transistors switch [23]. The bandwidth (BW) of the input impedance needed to be considered is determined by the exciting signal [24], which could be calculated with the rise time (rt) of the exciting signal as

$$BW = \frac{0.35}{rt} \tag{1}$$

The target impedance is given as follow

$$Z_T = \frac{V_{dd} \times \Delta ripple}{I_{transient}} \tag{2}$$

where V_{dd} is the power supply voltage of the PDN, $\Delta ripple$ is the allowed noise margin and $I_{transient}$ is the transient current. The transient characteristics of the SSN and switching current are not considered in the target impedance method, and the studies in [25–29] have shown that frequency-domain analysis is not accurate enough at the high-frequency domain and analysis in time domain is required.

The PDN circuit system can be simplified to a single resonance circuit model, as shown in Fig. 2, which consists of a resistor, an inductor, a capacitor, a VRM and a current source which represents the switching current. The capacitor is used to provide power to the current source, the VRM is the power supply, the resistor and the inductor are the spreading resistance and inductance from the power supply to the capacitor. The PDN impedance Z_{in} is the input impedance of the current source. So the PDN impedance Z_{in} is the parallel circuit of resistor, inductor and capacitor which can be represented in the Laplace domain as

$$Z_{in} = (SL + R) \,||\, \frac{1}{SC} = \frac{SL + R}{S^2LC + SCR + 1} \tag{3}$$

By inverse Laplace transformation, the time-domain impedance

function can be obtained as

$$z_{in}(t) = \frac{1}{C}\exp\left(-\frac{Rt}{2L}\right)\left[\cos\left(t\sqrt{\frac{1}{LC}-\left(\frac{R}{2L}\right)^2}\right) + \frac{R\sqrt{C}}{\sqrt{4L-R^2C}}\sin\left(t\sqrt{\frac{1}{LC}-\left(\frac{R}{2L}\right)^2}\right)\right]\varepsilon(t) \quad (4)$$

where $\varepsilon(t)$ is the unit step function. With $\theta = \arccos\left(1/\sqrt{\left(1+\frac{RC}{4L-R^2C}\right)}\right)$, Equation (4) can be rewritten as

$$z_{in}(t) = \frac{1}{C}\sqrt{\left(1+\frac{RC}{4L-R^2C}\right)}\exp\left(-\frac{Rt}{2L}\right)\cos\left(t\sqrt{\frac{1}{LC}-\left(\frac{R}{2L}\right)^2}+\theta\right)\varepsilon(t) \quad (5)$$

So the time-domain waveform of SSN could be calculated as

$$v(t) = -z_{in}(t) * i(t) \quad (6)$$

The digital signal and switching current waveforms are shown in Fig. 3. The width of switching current is the rise time or fall time of the digital signal, 10%–20% of the digital signal period. The switching current could be seen as an impulse signal with a limited magnitude if the main resonant frequencies of the PDN are small enough compared with the reciprocal of current pulse width. For typical PDNs, the width of switching current is in the order of 10^{-1} ns, and the resonant frequencies of the PDN are mainly in the order of 10^2 MHz. Because of $\int_{-\infty}^{\infty}\delta(t)dt = 1$, the integral of the switching current pulse can be obtained as

$$\int_{-\infty}^{\infty} i(t)dt = -S\int_{-\infty}^{\infty}\delta(t)dt \quad (7)$$

where S is the area of current pulse. So the switching current pulse can be substituted with $i(t) = -S\delta(t)$, and the time-domain waveform of SSN can be calculated as

$$v_{in}(t) = -\frac{1}{C}S\sqrt{\left(1+\frac{RC}{4L-R^2C}\right)}\exp\left(-\frac{Rt}{2L}\right)\cos\left(\sqrt{\frac{1}{LC}-\left(\frac{R}{2L}\right)^2}t+\theta\right)\varepsilon(t) \quad (8)$$

As shown in Equation (8), the SSN is a period function whose period could be calculated with $2\pi/\sqrt{\frac{1}{LC}-\left(\frac{R}{2L}\right)^2}$. For typical PDNs, the dc resistance R is very small and could be neglected, so the period

of the PDN could be estimated by $2\pi\sqrt{LC}$, which is consistent with the resonant frequency. The damping characteristic is introduced by the resistor and inductor which could be represented as $\exp(-R/2L)$, and the larger resistance results in shorter time to reach the steady state, nevertheless, larger inductance prevent the change of noise voltage. It could be concluded that the SSN characteristics are mainly determined by the resonant frequencies and the corresponding impedance values of the PDN. The performance of the circuit system is mainly limited by the magnitude of SSN and it is easily found that the largest magnitudes of the SSN are produced when $t_m = (m\pi - \theta)\sqrt{LC}$ $(m = N)$, which could be calculated as

$$v(t_m) = -\frac{1}{C} S \sqrt{\left(1 + \frac{RC}{4L - R^2C}\right)} \exp\left(-\frac{Rt_m}{2L}\right) \tag{9}$$

For periodic digital signal, the switching current period $T_{current}$ is the digital signal period, so the periodic SSN can be calculated as

$$v_{period}(t) = \sum_{r=0}^{+\infty} v_{in}(t - rT_{current}) \tag{10}$$

It is found that the SSN produced by one current pulse represents periodic characteristics, whose periods are mainly determined by the resonant frequencies of the PDN. For periodic switching current, the SSN is periodic accumulation of the noise waveforms produced by one current pulse based on the period of switching current, and the periods of the noise waveforms produced by one current pulse can be

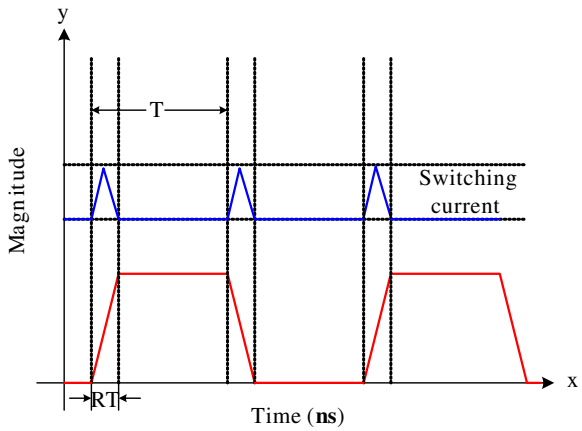

Figure 3. Digital signal voltage and switching current waveforms.

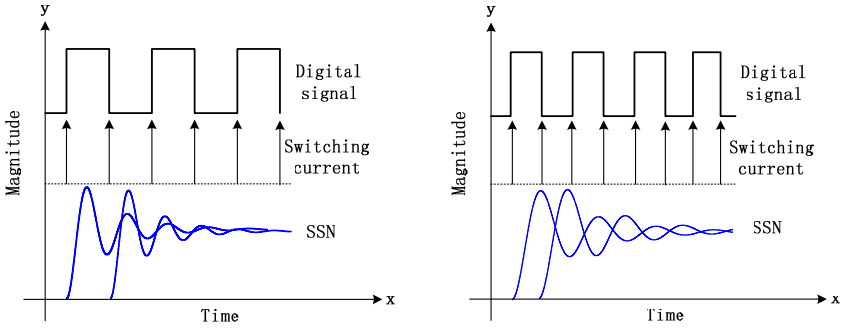

(a) $T_{current}$= (n+1)T_{noise} (b) $T_{current}$= (n+1/2)T_{noise}

Figure 4. Periodic characteristics of SSN produced by periodic switching current.

approximated as T_{noise}, which are mainly determined by the resonant frequencies. As shown in Fig. 4(a), the magnitude of SSN would accumulate positively with $T_{current} = (n+1)\,T_{noise}$ $(n = N)$, and as shown in Fig. 4(b), the magnitude of SSN would accumulate negatively with $T_{current} = (n+1/2)\,T_{noise}$ $(n = N)$. So SSN could be suppressed through changing the period of switching current and the resonant frequencies of the PDN. With $t_{2m} = (2m\pi - \theta)\sqrt{LC}(m = N)$, the worst case and the best case of SSN magnitudes produced by periodic switching current could be calculated as

$$v_{worst} = -\frac{1}{C}S\sum_{m=0}^{+\infty}\sqrt{\left(1+\frac{RC}{4L-R^2C}\right)}\exp\left(-\frac{Rt_{2m}}{2L}\right) \quad (11)$$

$$v_{best} = -\frac{1}{C}S\sum_{m=0}^{+\infty}\sqrt{\left(1+\frac{RC}{4L-R^2C}\right)}\exp\left(-\frac{Rt_{m}}{2L}\right) \quad (12)$$

2.2. SSN Estimation of the Multi-resonance Circuit

Generally, several resonance impedances may occur in a typical circuit system and the SSN characteristics are mainly determined by the resonant frequencies and the corresponding impedance values of the PDN. To capture the resonance characteristics, the PDN impedance of the multi-resonance circuit can be approximated with several single resonance circuits and represented as

$$Z_{in} = \sum_{n=1}^{N}\frac{SL_n + R_n}{S^2L_nC_n + SC_nR_n + 1} \quad (13)$$

where N is the number of the resonant frequencies, R_n, L_n and C_n are the resistor, inductor and capacitor parameters of the n-th resonant frequency. So the time-domain waveform of SSN can be calculated as

$$\begin{aligned} v_{in}(t) &= \sum_{n=1}^{N} -\frac{S}{C_n}\sqrt{\left(1+\frac{R_nC_n}{4L_n-R_n^2C_n}\right)}\exp\left(-\frac{R_nt}{2L_n}\right) \\ &\quad \cos\left(\sqrt{\frac{1}{L_nC_n}-\left(\frac{R_n}{2L_n}\right)^2}t+\theta_n\right)\varepsilon(t) \end{aligned} \tag{14}$$

where $\theta_n = \arccos\left(1/\sqrt{\left(1+\frac{R_nC_n}{4L_n-R_n^2C_n}\right)}\right)$. Based on the aforementioned analysis and neglecting the phase skew of SSN induced by different resonant frequencies, and with $t_n(m) = (m\pi-\theta_n)\sqrt{L_nC_n}$ $(m=N)$, the worst case and the best case of SSN produced by periodic switching current of the multi-resonance circuit could be calculated as

$$v_{worst} = \sum_{n=1}^{N}\left[-\frac{S}{C_n}\sum_{m=0}^{+\infty}\sqrt{\left(1+\frac{R_nC_n}{4L_n-R_n^2C_n}\right)}\exp\left(-\frac{R_nt_n(2m)}{2L_n}\right)\right] \tag{15}$$

$$v_{best} = \sum_{n=1}^{N}\left[-\frac{S}{C_n}\sum_{m=0}^{+\infty}\sqrt{\left(1+\frac{R_nC_n}{4L_n-R_n^2C_n}\right)}\exp\left(-\frac{R_nt_n(m)}{2L_n}\right)\right] \tag{16}$$

3. CALCULATION OF THE EQUIVALENT RESONANCE CIRCUIT PARAMETERS

The PDN could be supposed as a black box model, whose impedance frequency response could be captured with a rational function [30]. It is easily found that Equation (13) could be approximated as

$$\begin{aligned} Z_{in} &= c+\sum_{n=1}^{N}\frac{2k_{nr}(s-p_{nr})-2k_{ni}p_{ni}}{(s-p_{nr})^2+p_{ni}^2} \\ &= c+\sum_{n=1}^{N}\left(\frac{k_{nr}+jk_{ni}}{s-p_{nr}-jp_{ni}}+\frac{k_{nr}-jk_{ni}}{s-p_{nr}+jp_{ni}}\right) \end{aligned} \tag{17}$$

where the n-th poles $p_{nr}-jp_{ni}$, $p_{nr}+jp_{ni}$and corresponding residues $k_{nr}-jk_{ni}$, $k_{nr}+jk_{ni}$ are complex conjugate pairs, and the constant c is very small that could be neglected. Multiplying Equation (17) with a weighting function $\sigma(s) = 1+\sum_{n=1}^{2N}\frac{\tilde{k}_n}{s-\tilde{p}_n}$, Equation (17) is equivalent

to

$$c+\sum_{n=1}^{2N}\frac{k_n}{s-\bar{p}_n}=\sigma(s)\,Z(s)=\left[1+\sum_{n=1}^{2N}\frac{\tilde{k}_n}{s-\bar{p}_n}\right]Z(s) \tag{18}$$

where $\bar{p}_n$ is the starting pole of the weighting function and $\tilde{k}_n$ is the corresponding unknown residue, and $k_{nr}\pm jk_{ni}$ are expressed with k_n. Equation (18) can be rewritten as

$$Ax=b \tag{19}$$

where $A=\begin{bmatrix} \frac{1}{s_1-\bar{p}_1} & \cdots & \frac{1}{s_1-\bar{p}_{2N}} & 1 & \frac{-Z(s_1)}{s_1-\bar{p}_1} & \cdots & \frac{-Z(s_1)}{s_1-\bar{p}_{2N}} \\ \vdots & \vdots & \vdots & \vdots & \vdots & \vdots & \vdots \\ \frac{1}{s_m-\bar{p}_1} & \cdots & \frac{1}{s_m-\bar{p}_{2N}} & 1 & \frac{-Z(s_m)}{s_m-\bar{p}_1} & \cdots & \frac{-Z(s_m)}{s_m-\bar{p}_{2N}} \end{bmatrix}$, $x=\begin{bmatrix} k_1 & \cdots & k_{2N} & c & \tilde{k}_1 & \cdots & \tilde{k}_{2N} \end{bmatrix}^T$, $b=[Z(s_1)\cdots Z(s_m)]^T$, and s_m is the m-th sample of frequency. With enough frequency samples, Equation (19) can be solved as an over determined function using the least-squares solution. After obtaining the coefficient x, Equation (18) can be rewritten in pole-zero form

$$\frac{\prod_{n=1}^{2N}(s-z_n)}{\prod_{n=1}^{2N}(s-\bar{p}_n)}=\frac{\prod_{n=1}^{2N}(s-\tilde{z}_n)}{\prod_{n=1}^{2N}(s-\bar{p}_n)}Z(s) \tag{20}$$

where z_n and $\tilde{z}_n$ are the zeros computed by converting the pole-residue form to pole-zero form. So $Z(s)$ can be obtained as

$$Z(s)=\frac{\prod_{n=1}^{2N}(s-z_n)}{\prod_{n=1}^{2N}(s-\tilde{z}_n)} \tag{21}$$

The poles of $Z(s)$ are substituted with the zeros of $\sigma(s)$, $\tilde{z}_n$, and the poles converge to constant values by iteration. Substituting the new poles into Equation (17), a new matrix Equation (22) can be generated and solved with samples of frequency, where the unknown parameters contain the coefficients c and k_n as

$$\begin{bmatrix} 1 & \frac{1}{s_1-\tilde{z}_1} & \cdots & \frac{1}{s_1-\tilde{z}_{2N}} \\ \vdots & \vdots & \vdots & \vdots \\ 1 & \frac{1}{s_m-\tilde{z}_1} & \cdots & \frac{1}{s_m-\tilde{z}_{2N}} \end{bmatrix}\begin{bmatrix} c \\ k_1 \\ \vdots \\ k_{2N} \end{bmatrix}=\begin{bmatrix} Z(s_1) \\ \vdots \\ \vdots \\ Z(s_m) \end{bmatrix} \tag{22}$$

The frequency-domain impedance can be approximated with a rational function as Equation (17). Neglecting the constant c, the time-domain impedance function can be easily obtained by inverse Laplace transformation and the time-domain waveform of SSN can be calculated based on the characteristics of switching current as

$$v(t) = -2S \sum_{n=1}^{N} e^{p_{nr}t} \sqrt{\left(k_{nr}^2 + k_{ni}^2\right)} \cos\left(p_{ni}t + \theta_n\right) \varepsilon(t) \tag{23}$$

where $\theta_n = \arccos \frac{k_{nr}}{\sqrt{\left(k_{nr}^2+k_{ni}^2\right)}}$. The magnitude of noise is determined by the real parts and imaginary parts of residues k_{nr} and k_{ni}. The damping in transient response is introduced by the real parts of poles p_{nr}. The period of the noise is determined by the imaginary parts of poles p_{ni}, which are consistent with the resonant frequencies. All characteristic parameters of time-domain waveform are included in Equation (23), so the noise of PDNs could be expressed with it. With $t_n(m) = (m\pi - \theta_n)/p_{ni}$, the worst case and the best case of SSN could also be obtained as

$$v_{worst} = -2S \sum_{n=1}^{N} \sum_{m=0}^{+\infty} \sqrt{\left(k_{nr}^2 + k_{ni}^2\right)} \exp\left(p_{nr} t_n(2m)\right) \tag{24}$$

$$v_{best} = -2S \sum_{n=1}^{N} \sum_{m=0}^{+\infty} \sqrt{\left(k_{nr}^2 + k_{ni}^2\right)} \exp\left(p_{nr} t_n(m)\right) \tag{25}$$

4. EXPERIMENTAL VALIDATIONS OF SIMULTANEOUS SWITCHING NOISE ESTIMATION

4.1. Single Resonance Lumped Circuit Model of the Power Delivery Network

The lumped circuit model of a PDN is modeled in Hspice and shown in Fig. 5, the pins of the package, PCB and VRM are modeled with series inductor and resistor. The parameters of decoupling capacitors for providing power to IC and parasitic parameters of pins are shown in this figure. The decoupling capacitors are representd by the series of resistors, inductors and capacitors, where the parameters of resistors are the equivalent series resistances, the parameters of inductors are the equivalent series inductances, the parameters of capacitors are the capacitances. The current source is a triangle current pulse that has an amplitude of 1 A, a rise/fall time of 0.3 ns and the period of switching current is a variable parameter, so the bandwidth of the frequency-domain impedance should be considered is 1.17 GHz. The allowed

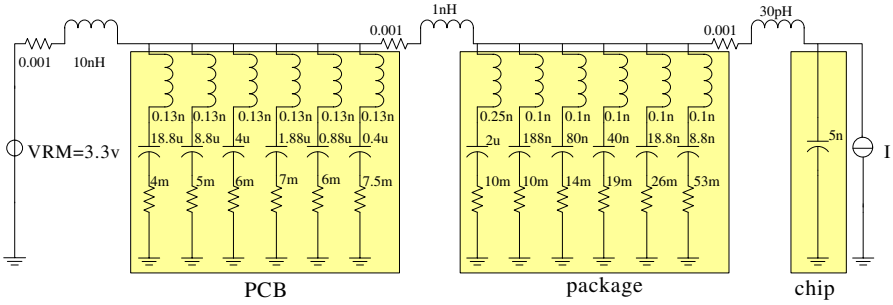

Figure 5. Typical system-level lumped circuit model of the PDN, including PCB, package, and chip.

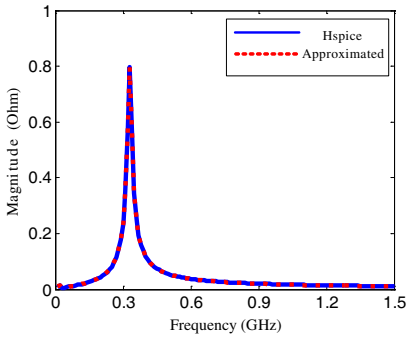

Figure 6. Input impedance of the PDN.

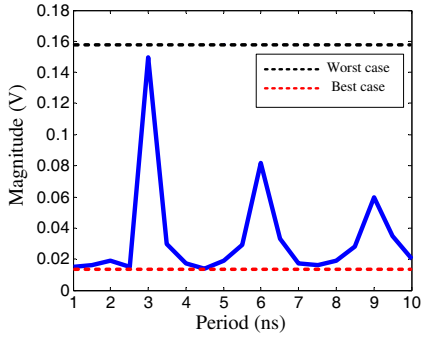

Figure 7. Comparison of the Hspice simulations with estimated results.

noise margin $\Delta ripple$ is set as 5%, so the target impedance could be calculated as 0.165 Ω. The simulated frequency-domain impedance of Hspice and the approximated result with the rational function are shown in Fig. 6, which are consistent with each other. The obtained poles and residues of the approximated result are $-6.03 \times 10^7 \pm j2.07 \times 10^9$ and $4.81 \times 10^7 \mp j2.19 \times 10^6$ respectively. The resonant frequency of the PDN is 330 MHz, so the period of SSN produced by one current pulse is 3 ns. The switching current is launched at chip pin whose period is changed from 1 ns to 10 ns and the corresponding digital signal speed is from 1 Gbps to 100 Mbps. The simulated SSN magnitudes of the steady state are shown in Fig. 7, in which the calculated worst case and the best case of SSN magnitudes with the proposed method are also shown, which are 0.158v and 0.014v respectively The simulated

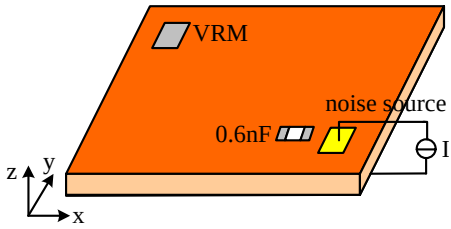

Figure 8. Distributed circuit model of a PCB.

largest and the smallest SSN magnitudes are 0.15v and 0.014v, which are consistent with the proposed method and lie between the values of the worst case and the best case. It is shown that the proposed method can estimate the largest and the smallest SSN magnitudes effectively and is accurate for the single resonance circuit. It is also found that the noise magnitude peaks are induced at $T_{current} = 3$ ns, $T_{current} = 6$ ns and $T_{current} = 9$ ns, which are the integral multiple period of the SSN produced by one current pulse, and the valleys of noise magnitudes are produced when SSN accumulates out phase, which is consistent with the aforementioned periodic characteristic analysis. It is easily found that the target impedance is not met, but the magnitude of the SSN is lower than the allowed noise, so the proposed method is more accurate than the target impedance method.

4.2. Multi-Resonance Distributed Circuit Model of the Printed Circuit Board

A distributed circuit model of a PCB with dimensions of 100 mm×80 mm is modeled in Hspice and shown in Fig. 8, the noise source and VRM are located at (90 mm, 10 mm) and (10 mm, 70 mm) respectively. The DC voltage of VRM is 3.3v, and the triangle current pulse source has an amplitude of 1 A, a rise/fall time of 0.3 ns and the period of switching current is a variable parameter, so the bandwidth of the frequency-domain impedance should be considered is 1.17 GHz. A 0.6 nF capacitor is used to model the capacitance on chip and place close to the noise source for suppressing the noise transmission. The simulated frequency-domain impedance of Hspice and the approximated results with the rational function are shown in Fig. 9, in which a good agreement is seen between them. The resonant frequencies of the PDN are 130 MHz and 390 MHz, so the periods of SSN produced by one current pulse could be approximated as 7.7 ns and 2.6 ns respectively The obtained poles and residues of the approximated result for 130 MHz resonant frequency are

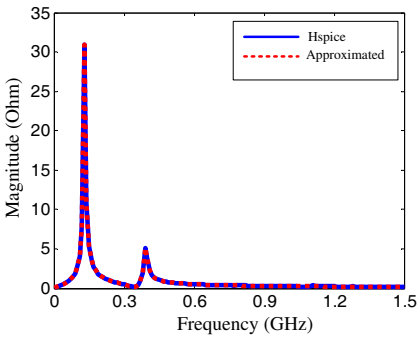

Figure 9. Input impedance of the PDN.

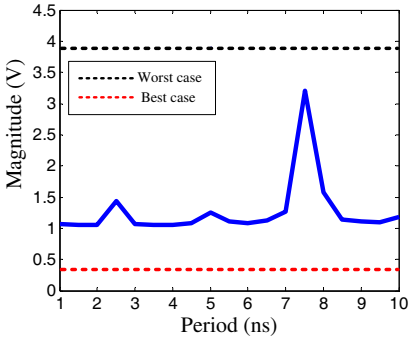

Figure 10. Comparison of the Hspice simulations with estimated results.

$-1.70 \times 10^7 \pm j8.26 \times 10^8$ and $6.02 \times 10^8 \pm j1.00 \times 10^7$ and the obtained poles and residues of the approximated result for 390 MHz resonant frequency are $-3.57 \times 10^7 \pm j2.46 \times 10^9$ and $1.97 \times 10^8 \mp j9.02 \times 10^6$ respectively. The switching current is launched at the noise source, whose period is changed from 1 ns to 10 ns, and the corresponding digital signal speed is from 1 Gbps to 100 Mbps. The simulated SSN magnitudes of the steady state are shown in Fig. 10 and the calculated worst case and the best case of SSN magnitudes with the proposed method are also shown in Fig. 10, which are 3.9v and 0.34v respectively. The simulated largest and the smallest SSN magnitudes are 3.25v and 1.05v, which are consistent with the proposed method and lie between the values of the worst case and the best case. The difference between the estimated results and simulated results is mainly attributed to the phase offset of the two different resonant frequencies. It shows that the proposed method can estimate the largest and the smallest SSN magnitudes effectively and is accurate for the multi-resonance circuit. It is also found that the noise magnitude peaks are induced at integral multiple periods of the SSN produced by one current pulse, $T_{current} = 2.6$ ns, $T_{current} = 5.2$ ns and $T_{current} = 7.7$ ns, which is consistent with the aforementioned periodic characteristic analysis. If the target impedance is set as the largest impedance value 31Ohm in Fig. 9, then the allowed noise would be 31v, which is not consistent with the simulated noise results, and the proposed method is more accurate than the target impedance method. It is obvious that the target impedance method would result in over design of the PDN because the transient characteristics of SSN produced by one current pulse and switching current are not considered.

5. CONCLUSION

In this paper, a new method is proposed to estimate the SSN directly from the PDN frequency-domain impedance based on the periodic characteristics of switching current and SSN produced by one current pulse because that the PDN frequency-domain impedance is much easier to obtain. The periodic characteristics of the SSN are discussed with simplified single resonance circuit model in details, which shows that the SSN characteristics are mainly determined by the resonant frequencies of the PDN. The worst case and the best case of SSN are calculated by approximating the PDN frequency-domain impedance with the rational function. The performance of the new method for estimating the SSN is verified with the single resonance lumped circuit model and multi-resonance distributed PDN model, which is more accurate than the target impedance method.

ACKNOWLEDGMENT

This work was supported by the National Natural Science Foundation of China under Contract 60672027 and 60871072, Planned Science and Technology Project of Hunan Province 2010FJ6015, Hunan Provincial Natural Science Foundation of China 10JJ609.

REFERENCES

1. Huang, W. T., C. H. Lu, and D. B. Lin, "Suppression of crosstalk using serpentine guard trace vias," *Progress In Electromagnetics Research*, Vol. 109, 37–61, 2010.
2. Marynowski, W., P. Kowalczyk, and J. Mazur, "On the characteristic impedance definition in microstrip and coplanar lines," *Progress In Electromagnetics Research*, Vol. 110, 219–235, 2010.
3. Lin, D. B., F. N. Wu, W. S. Liu, C. K. Wang, and H. Y. Shih, "Crosstalk and discontinuities reduction on multi-module memory bus by particle swarm optimization," *Progress In Electromagnetics Research*, Vol. 121, 53–74, 2011.
4. Sharma, R., T. Chakravarty, and A. B. Bhattacharyya, "Reduction of signal overshoots in high-speed interconnects using adjacent ground tracks," *Journal of Electromagnetic Waves and Applications*, Vol. 24, No. 7, 941–950, 2010.
5. Xie, H., J. Wang, R. Fan, and Y. Liu, "Spice models for radiated and conducted susceptibility analyses of multiconductor shielded

cables," *Progress In Electromagnetics Research*, Vol. 103, 241–257, 2010.

6. Lim, H. and N. H. Myung, "A novel hybrid Aipo-MoM technique for jet engine modulation analysis," *Progress In Electromagnetics Research*, Vol. 104, 85–97, 2010.
7. Mirzavand, R., A. Abdipour, G. Moradi, and M. Movahhedi, "CFS-PML implementation for the unconditionally stable FDTD method," *Journal of Electromagnetic Waves and Application*, Vol. 25, No. 5–6, 879–888, 2011.
8. Chen, C. Y., Q. Wu, X. J. Bi, Y. M. Wu, and L. W. Li, "Characteristic analysis for FDTD based on frequency response," *Journal of Electromagnetic Waves and Application*, Vol. 24, No. 2–3, 282–292, 2010.
9. Lee, K., H. I. Ahmed, R. S. M. Goh, E. H. Khoo, E. P. Li, and T. G. G. Hung, "Implementation of the FDTD method based on Lorentz-Drude dispersive model on Gpu for plasmonics applications," *Progress In Electromagnetics Research*, Vol. 116, 441–456, 2011.
10. Izadi, M., M. Z. A. Ab Kadir, and C. Gomes, "Evaluation of electromagnetic fields associated with inclined lightning channel using second order FDTD-hybrid methods," *Progress In Electromagnetics Research*, Vol. 117, 209–236, 2011.
11. Ling, J., S. X. Gong, S. T. Qin, W. T. Wang, and Y.-J. Zhang, "Wide-band analysis of on-platform antenna using MoM-PO combined with Maehly approximation," *Journal of Electromagnetic Waves and Applications*, Vol. 24, No. 4, 475–484, 2010.
12. Trujillo-Romero, C. J., L. Leija, and A. Vera, "FEM modeling for performance evaluation of an electromagnetic oncology deep hyperthermia applicator when using monopole, inverted T, and plate antennas," *Progress In Electromagnetics Research*, Vol. 120, 99–125, 2011.
13. Li, W. D., J. X. Miao, J. Hu, Z. Song, and H. X. Zhou, "An improved cubic polynomial method for interpolating/extrapolating MoM matrices over a frequency band," *Progress In Electromagnetics Research*, Vol. 117, 267–281, 2011.
14. Kim, J. H. and M. Swaminathan, "Modeling of irregular shaped power distribution planes using transmission matrix method," *IEEE Transactions on Advanced Packaging*, Vol. 24, No. 3, 334–346, 2001.
15. Kim, H., Y. Jeong, J. Park, S. Lee, J. Hong, and Y. Hong, "Significant reduction of power/ground inductive impedance and

simultaneous switching noise by using embedded film capacitor," *Electr. Perform Electron Package*, 129–132, 2003.

16. Hobbs, J. M., H. Windlass, V. Sundaram, S. Chun, G. E. White, M. Swaminathan, and R. R. Tummala, "Simultaneous switching noise suppression for high speed systems using embedded decoupling," *Proceeding Electron. Comon. Technol. Conference 2001*, 339–343, 2001.
17. Kim, S. H., T. T. Nguyen, and J. H. Jang, "Reflection characteristics of 1-D EBG ground plane and its application to a planar dipole antenna," *Progress In Electromagnetics Research*, Vol. 120, 51–66, 2011.
18. He, Y., L. Li, C. H. Liang, and Q. H. Liu, "EBG structures with fractal topologies for ultra-wideband ground bounce noise suppression," *Journal of Electromagnetic Waves and Applications*, Vol. 24, No. 10, 1365–1374, 2010.
19. Tomeo-Reyes, I. and E. Rajo-Iglesias, "Comparative study on different His as ground planes and its application to low profile wire antennas design," *Progress In Electromagnetics Research*, Vol. 115, 55–77, 2011.
20. Jandieri, V., K. Yasumoto, and Y. K. Cho, "Rigorous analysis of electromagnetic scattering by cylindrical EBG structures," *Progress In Electromagnetics Research*, Vol. 121, 317–342, 2011.
21. Hubing, T., J. Chen, J. Drewnik, T. V. Doren, Y. Ren, J. Fan, and R. E. DuBroff, "Power bus noise reduction using power island in printed circuit board designs," *Proc. Int. Symp. Electromagn. Compat. 1999*, 1–4, 1999.
22. Wu, T. L., S. T. Chen, J. N. Huang, and Y. H. Lin, "Numerical and experimental investigation of radiation caused by the switching noise on the partitioned dc power/ground-planes of high-speed digital PCB," *IEEE Trans Electromagnetic Compatibility*, Vol. 46, 33–45, 2004.
23. Smith, L. D., R. E. Anderson, D. W. Forehand, T. J. Pelc, and T. Roy, "Power distribution system design methodology and capacitor selection for modern CMOS technology," *IEEE trans. Advanced Package*, Vol. 22, 284–291, 1999.
24. Eric, B., *Signal Integrity-Simplified*, 59–61, Prentice Hall PTR, 2003.
25. Eudes, T., B. Ravelo, and A. Louis, "Transient response characterization of the high-speed interconnection rlcg-model for the signal integrity snalysis," *Progress In Electromagnetics Research*, Vol. 112, 183–197, 2011.

26. Ding, T. H., Y. S. Li, X. Yan, and Y. Z. Qu, "A new efficient method for calculation and suppression of simultaneous switching noise with the time-domain impedance function for high-speed circuit design," *Progress In Electromagnetics Research*, Vol. 112, 41–62, 2011.
27. Klopf, E. M., S. B. Manić, M. M. Ilic, and B. M. Notaros, "Efficient time-domain analysis of waveguide discontinuities using higher order FEM in frequency domain," *Progress In Electromagnetics Research*, Vol. 120, 215–234, 2011.
28. Drewniak, J. L., et al., "Comparing time-domain and frequency domain techniques for investigation on charge delivery and power-bus noise for high-speed printed circuit boards," *Design Con.*, 2007.
29. Cheng, W. L., A. Sarkar, S. Lin, and J. Zheng "Worst case switching pattern for core noise analysis," *Design Con.*, 2009.
30. Gustavsen, B. and A. Semlyen, "Rational approximation of frequency response by vector fitting," *IEEE Transactions on Power Delivery*, Vol. 14, 1052–1061, 1999.